Stability of plane Couette flow under anisotropic superhydrophobic effects

Liheng Zhang(张立恒)*[1], Xueyan Zhai(翟雪艳)*[1], Baofang Song(宋保方)†[2], and Yaohong Wang(王耀宏)[1]

[1]Center for Applied Mathematics, Tianjin University, Tianjin 300072, China
[2]State Key Laboratory of Turbulence and Complex Systems, College of Engineering, Peking University, Beijing 100871, China

Abstract

We study the linear stability of plane Couette flow subject to an anisotropic slip boundary condition that models the slip effect of parallel microgrooves with a misalignment about the direction of the wall motion. This boundary condition has been reported to be able to destabilize channel flow far below the critical Reynolds number of the no-slip case. Unlike channel flow, the no-slip plane Couette flow is known to be linearly stable at arbitrary Reynolds numbers. Nevertheless, the results show that the slip can cause linear instability at finite Reynolds numbers also. The misalignment angle of the microgrooves that maximizes the destabilizing effect is nearly $\pi/4$, and the unstable modes are of small streamwise wavenumbers and relatively large spanwise wavenumbers. The flow is always more destabilized by two slippery walls compared to a single slippery wall. These observations are in qualitative agreement with the slippery channel flow with the same boundary condition, indicating that such an anisotropic superhydropbobic effect has a rather general destabilizing effect in shear flows regardless of the profile of the base flow. The absence of the Tollmien-Schlichting instability allows us to reveal the inverse relationship between the critical Reynolds number and the slip length as well as the misalignment in the small-parameter regime. The results suggest that arbitrary nonvanishing slip length and misalignment, with arbitrarily weak anisotropy, may suffice to destabilize plane Couette flow.

1 Introduction

On a smooth solid surface, a viscous fluid sticks to the surface (on macroscopic scale) and a no-slip boundary condition is the natural choice. On the other hand, superhydrophobic solid surfaces can induce an apparent velocity slip in viscous flows (see e.g. Refs. [1–7]). This effect can be modeled as a partial slip on a smooth solid surface with proper slip parameters, following the spirit of the Navier-slip boundary condition. This simplification avoids treating the complex microstructures of the solid surface, easing computational and theoretical analysis, and has been applied to a broad range of problems including linear stability [8–24], transition and turbulence [20, 21, 23, 25, 26]. The focus of this paper is the linear stability problem.

The simplest slip boundary condition is a Robin-type condition on velocity with a single slip length parameter. This essentially assumes isotropy and homogeneity in the surface properties, i.e. slip properties are independent of the direction and location within the solid surface. In this case, studies have shown that the flow is stabilized by the velocity slip [8, 10, 11, 13, 18, 19, 27]. For example, in channel flow, the two dimensional (2D) Tollmien-Schlichting modes (T-S modes), which are the dominant linear modes,

*These authors contributed equally to this work
†Email address for correspondence: baofang.song@pku.edu.cn

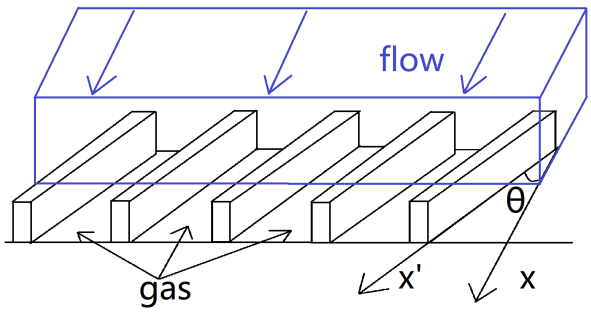

Figure 1: Schematic of the liquid flow over a microgrooved superhydrophobic surface. The x axis shows the flow direction (i.e. the direction of the driving pressure gradient in case of channel flow and the direction of wall motion in the plane Couette flow case), and x' shows the longitudinal direction of the microgrooves. The misalignment angle is denoted as θ.

have been shown to be significantly stabilized by the slip so that the critical Reynolds number for linear instability is higher than the classic no-slip case [18, 19, 23]. Similarly, slip was shown to delay natural transition in boundary layer flow by stabilizing the 2D T-S modes [21]. We want to note here that the above-mentioned stabilizing effect was concluded for single-phase parallel shear flows. In the case of nonparallel flows (such as divergent channel flow) and multiphase flows with interfaces or viscosity stratification, slip can have a destabilizing effect also [12, 16, 17]. In this paper, we only discuss about single-phase parallel shear flows.

In contrast, if anisotropy is introduced to the slip effect, it was shown that the slip does not always stabilize the flow but can also destabilize the flow given proper parameters [18, 19, 22, 23, 27]. The simplest situation is channel flow with distinct slip lengths in the streamwise and spanwise directions [19, 27]. The anisotropy was shown to be able to destabilize three dimensional (3D) perturbations at much lower Reynolds numbers than the critical Reynolds number for 2D T-S modes. Such slip effect can be generated by superhydrophobic surfaces with textures that have distinct geometric properties in different directions, such as parallel microgrooves. It can be expected that the slip effect would be different in the longitudinal and transverse directions for microgrooves, which indeed is the case according to several theoretical analysis [28, 29]. The slip length in the longitudinal direction was shown to be larger than that in the transverse direction. In this paper, we will focus on this type of superhygrophobic surface considering that it is possibly the easiest way to introduce anisotropy in experiments.

Besides different slip lengths in different directions, microgrooves can have a misalignment about the driving direction (e.g. pressure gradient in channel flow and wall motion in plane Couette flow), which adds further complexity to the slip effect (see Fig. 1). According to theoretical analysis, this complexity can be modeled with a tensorial slip boundary condition [18, 28, 30]

$$\begin{bmatrix} u \\ w \end{bmatrix} + \Lambda \frac{\partial}{\partial n} \begin{bmatrix} u \\ w \end{bmatrix} = 0 \tag{1}$$

at the walls, where u denotes the velocity component along the direction of the top-wall motion (will be referred to as streamwise direction for simplicity), w denotes the spanwise velocity, and n denotes the outward normal direction at the wall. It should be noted that u and w should be the velocities relative to the solid wall when considering slip boundary condition. The boundary condition for the wall normal velocity is $v = 0$. The slip properties are given by the tensor Λ with the following form

$$\boldsymbol{\Lambda} = \boldsymbol{Q} \begin{bmatrix} \lambda^{\parallel} & 0 \\ 0 & \lambda^{\perp} \end{bmatrix} \boldsymbol{Q}^T, \text{ with } \boldsymbol{Q} = \begin{bmatrix} \cos\theta & -\sin\theta \\ \sin\theta & \cos\theta \end{bmatrix}, \tag{2}$$

where $\lambda^{\parallel}$ and $\lambda^{\perp}$ correspond to the slip lengths in the longitudinal and transverse directions, respectively, and θ is the angle of misalignment of the microgrooves about the driving direction (this direction will be

referred to as the streamwise direction hereafter). The two slip lengths can be determined by the specific geometries of the microgrooves [29].

There is certainly a limitation of the applicability of the above homogenization of the surface and base flow. The global stability analysis of Ref. [31, 32] considering the actual structure of the textured surface showed that the above homogenization only applies when the texture periodicity L (transverse periodicity of the grooves) is much smaller compared to the distance between the two walls H (the gap width). When $L/H = O(0.01)$, the global stability analysis and the local stability analysis with homogenization treatment give very close results. However, when $L/H = 0.1$, the base flow cannot be homogenized, and the spanwise alteration of solid and gas parts causes an inflectional instability of the base flow, which can occur at much lower Reynolds number compared to the homogenized case [31]. Other types of inviscid instability have also been reported when L/H is large [32]. Besides, by considering the interface dynamics on the liquid-gas interface, Ref. [23, 33] showed that an interfacial instability can occur when $L/H = O(0.1)$ or larger, which can become the dominant destabilizing mechanism, whereas $L/H = O(0.01)$ or smaller does not suffer this problem no matter the value of the shear-free portion δ of the surface. Therefore, we only consider the case $L/H = O(0.01)$ or smaller where the grooved surface can be homogenized with the slip boundary condition (1).

With this boundary condition, a few studies investigated the effects of the slip anisotropy and misalignment on the critical Reynolds numbers for linear instability in channel flow [18, 24]. The results show that the slip can significantly destabilize the flow and cause linear instability at Reynolds numbers much below the critical Reynolds number of the no-slip case. The Squire's theorem may not hold anymore and 3D perturbations can become the most dangerous ones [18], depending on the specific parameters, and the lowest critical Reynolds number is realized for 3D perturbations at the misalignment somewhere around $\theta = \pi/4$. The larger the anisotropy (quantified by the slip length ratio $\lambda^{\parallel}/\lambda^{\perp}$), the more the flow is destabilized (i.e. the lower the critical Reynolds number), and in most cases, channel flow with two superhygrophobic walls is more unstable than that with a single slippery wall [24]. More complicated behaviors may appear in the small-misalignment and small-slip-length regimes due to the competition between the T-S instability and the instability caused by the slip [24]. Recently, Ref. [23] studied the stability and transition to turbulence in channel flow with the same boundary condition and confirmed the destabilizing effects of the slip. All these studies [18, 23, 24] showed that the 3D superhydrophobic instability modes are of small streamwise wavenumbers and relatively large spanwise wavenumbers, which is similar to the crossflow instability in 3D boundary layer flows [34, 35]. Therefore, this raises the question whether the superhydrophobic instability is caused by the cross-flow component of the base flow induced by the slip and belongs to the cross-flow instability. But unlike the 3D boundary layer flow, in which the cross-flow component is inflectional and responsible for the cross-flow instability, it was pointed out that the cross-flow component in channel flow induced by the slip boundary condition (1) is either constant or linear and therefore is not inflectional [18, 23, 24]. It is still unclear how a non-inflectional base flow can induce the seeming cross-flow instability, or if the cross-flow component of the base flow does not take part in the instability at all. The destabilizing mechanism remains to be clarified.

Distinct with channel flow, the no-slip plane Couette flow has been rigorously proved to be linearly stable at arbitrary Reynolds numbers [36, 37]. The aim of this paper is to study the slip effect on the stability of plane Couette flow and to find out whether such an anisotrpopic boundary condition can also induce a linear instability or not. The effects of the slip on the eigenspectrum and the dependence of the critical Reynolds number on the slip parameters will be studied particularly. Due to the absence of the T-S instability in plane Couette flow, the flow must behave differently in the small-misalignment and small-slip-length regimes, which will be discussed also.

It should be noted that, in shear flows, non-modal instability usually plays a more important role than modal instability in transition to turbulence if perturbation level is sufficiently high. Specific to plane Couette flow, it has been shown that transition can occur at Reynolds numbers of a few hundreds under finite-amplitude perturbations (see, e.g. [38, 39]). Linear modal stability analysis certainly cannot cover all aspects of flow stability, especially for no-slip plane Couette flow which is always linearly stable.

Nevertheless, as reported in Ref. [23], the linear instability incurred by this anisotropic slip effect opens a new route to turbulence when velocity-perturbation level is low, especially when the non-modal growth of small perturbations is not sufficient for triggering the transition. If the slip could also destabilize plane Couette flow also, there will be an alternative route to turbulence as well. Besides, the destabilizing effect of the slip could be utilized to enhance transport and mixing processes in flows. The major point of this work is to first clarify whether this anisotropic effect has a general destabilizing effect on shear flows, disregarding the properties of the basic flow.

2 Methods

2.1 The physical model and linearized equations

We consider the nondimensional incompressible Navier-Stokes equations for a plane Couette flow in Cartisian coordinates (x, y, z), where $\boldsymbol{u} = (u, v, w)$ denotes the velocity and p denotes the pressure. The flow is driven by the walls moving in opposite directions at speeds U_w and $-U_w$, respectively. Velocities are normalized by U_w, length by half gap width h and time by h/U_w, and the Reynolds number $Re = U_w h/\nu$ where ν is the kinematic viscosity of the fluid. The origin of the y-axis is placed at the centreplane.

In the following, we denote the fully developed base flow as

$$\boldsymbol{U} = U(y)\boldsymbol{e}_x + W(y)\boldsymbol{e}_z, \tag{3}$$

where $\boldsymbol{e}_x$ and $\boldsymbol{e}_z$ are the unit vectors in the streamwise and spanwise directions, respectively. The governing equations for U and W are

$$\frac{\mathrm{d}^2 U}{\mathrm{d}y^2} = 0, \quad \frac{\mathrm{d}^2 W}{\mathrm{d}y^2} = 0. \tag{4}$$

Subject to the slip boundary condition (1), the base flow in case of a single SH wall, say the bottom wall, reads

$$U(y) = \frac{k\lambda^2 + 2\lambda(k\sin^2\theta + \cos^2\theta)}{k\lambda^2 + 2(k+1)\lambda + 4}(1-y) + y, \tag{5}$$

$$W(y) = \frac{2(1-k)\lambda\sin\theta\cos\theta}{k\lambda^2 + 2(k+1)\lambda + 4}(1-y), \tag{6}$$

where $\lambda := \lambda^{\parallel}$ and $k = \lambda^{\perp}/\lambda^{\parallel}$ is the slip length ratio. If both walls are slippery and assuming the same slip parameters on the two walls, the base flow reads

$$U(y) = \left(1 - \frac{k\lambda^2 + \lambda\cos^2\theta + k\lambda\sin^2\theta}{(k\lambda+1)(\lambda+1)}\right) y, \tag{7}$$

$$W(y) = \frac{(1-k)\lambda\sin\theta\cos\theta}{(k\lambda+1)(\lambda+1)} y. \tag{8}$$

In either case, both the U and W components of the base flow are linear with respect to y and the wall-normal component of the base flow is $V = 0$ considering the impermeability condition at the walls.

Introducing small disturbances $\boldsymbol{u} = (u, v, w)$ and linearizing the Navier-Stokes equations about the base flow, we obtain the governing equation for $\boldsymbol{u}$ as the following,

$$\frac{\partial \boldsymbol{u}}{\partial t} + \boldsymbol{u}\cdot\boldsymbol{\nabla}\boldsymbol{U} + \boldsymbol{U}\cdot\boldsymbol{\nabla}\boldsymbol{u} = -\boldsymbol{\nabla}p + \frac{1}{Re}\boldsymbol{\nabla}^2\boldsymbol{u}, \quad \nabla\cdot\boldsymbol{u} = 0 \tag{9}$$

with the condition Eqs. (1) and impermeability condition for $\boldsymbol{u}$. In the following, we introduce primitive variable formulation for the eigenvalue analysis. Alternatives such as velocity-vorticity formulation and

time-stepping the Navier-Stokes equations can also be used [24]. A disturbance is expressed in terms of Fourier modes along the wall-parallel directions,

$$q(x,y,z,t) = \hat{q}(y)e^{i(\alpha x+\beta z-\omega t)} + c.c., \tag{10}$$

where α and β are the streamwise and spanwise wavenumbers, respectively, $\hat{q}$ is the Fourier coefficient, and c.c. denotes the complex conjugate. The complex angular frequency is denoted as $\omega = \omega_r + i\omega_i$ (subscript i denotes the imaginary part, and subscript r denotes the real part) and $\omega_i > 0$ indicates a linear instability. Plugging into Eqs. (9), we get

$$-i\omega \boldsymbol{B}\hat{\boldsymbol{q}} = \boldsymbol{L}\hat{\boldsymbol{q}}. \tag{11}$$

This is an generalized eigenvalue problem, where

$$\boldsymbol{B} = \begin{bmatrix} 1 & 0 & 0 & 0 \\ 0 & 1 & 0 & 0 \\ 0 & 0 & 1 & 0 \\ 0 & 0 & 0 & 0 \end{bmatrix}, \quad \boldsymbol{L} = \begin{bmatrix} A & -\frac{\partial U}{\partial y} & 0 & -i\alpha \\ 0 & A & 0 & -\frac{\partial}{\partial y} \\ 0 & -\frac{\partial W}{\partial y} & A & -i\beta \\ i\alpha & \frac{\partial}{\partial y} & i\beta & 0 \end{bmatrix}, \quad \hat{\boldsymbol{q}} = \begin{bmatrix} \hat{u} \\ \hat{v} \\ \hat{w} \\ \hat{p} \end{bmatrix}, \tag{12}$$

$$A = \frac{1}{Re}(\frac{\partial^2}{\partial y^2} - \alpha^2 - \beta^2) - i\alpha U - i\beta W. \tag{13}$$

We use a Chebyshev-collocation discretization in the wall-normal direction [40]. This formulation has been validated against velocity-vorticity formulation and time-stepping the linearized Navier-Stokes equations for channel flow, and the readers are referred to Ref. [24] for details about the validation and numerical methods.

3 Results

First, we make a note on the selection of the value of the slip length λ in this study. As discussed in the introduction, we choose the groove periodicity to channel gap width ratio $L/H = O(0.01)$ so that the homogenization of the wall surface and the local stability analysis apply [31, 32]. The slip length λ has been estimated to be up to $0.02 \sim 0.03$ with the groove periodicity $L = 0.02 \sim 0.025$ and the gas fraction up to $\delta = 0.9$ [23, 31]. Larger λ is possible in principle if δ is larger, and λ could even approach infinity in theory if $\delta \to 1$ and the liquid protrudes into the grooves [41]. However, it may be difficult to achieve and maintain very large δ in experiments, and $\lambda = O(0.01)$ or smaller should be considered realistic. Nevertheless, in this paper, λ is taken up to around 0.1 mainly for illustrative purposes (e.g. to show the trend) and to compare with the results for channel flow in some studies where λ is taken up to above 0.1 [18, 19, 24, 27].

3.1 Effects of the anisotropic slip on the eigenvalues

We show the effect of the slip on the distribution of ω_i in the $\alpha - \beta$ plane, and only the one-SH-wall case will be considered for this study. In the no-slip case, the distribution of ω_i is symmetric about either the $\alpha = 0$ or $\beta = 0$ axis, see figure 2(a), therefore, only a single quadrant, say the first quadrant, needs to be considered for the linear stability analysis. The flow is stable at arbitrary Re and the $(\alpha, \beta) = (0, 0)$ mode is the least stable mode. On the contrary, in the slip case, it can be seen from figure 2(b,c) that the distribution is not symmetric about either axis anymore, therefore, a half plane needs to be considered for the stability analysis. The instability appears in a region with small α and relatively large $|\beta|$. As the slip length increases, the unstable region enlarges and ω_i increases as well. Therefore, it can be concluded that the slip has a destabilizing effect to the flow. Similar observations have been reported for channel flow [23]. However, in channel flow, there would be an unstable TS-mode region that is least stable or

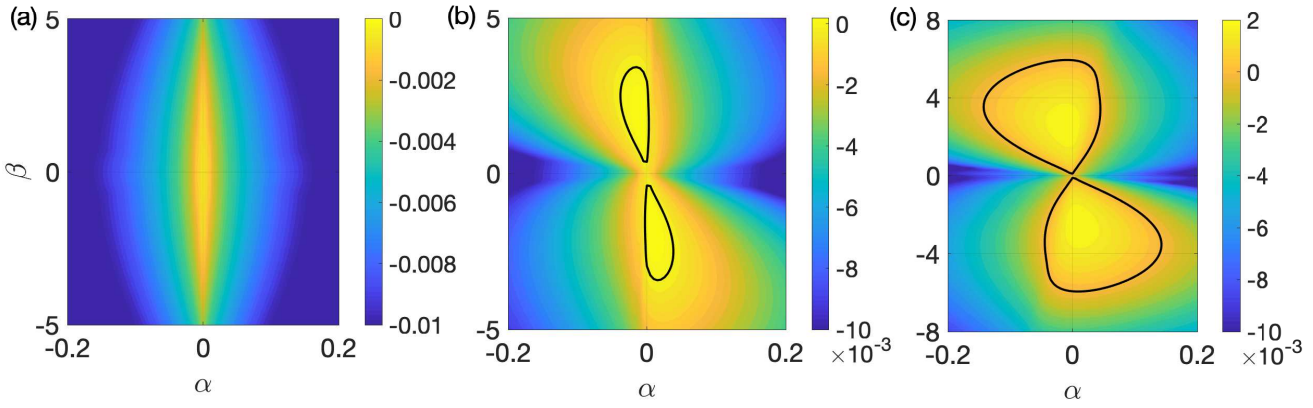

Figure 2: The distribution of ω_i in the $\alpha - \beta$ plane for $Re = 5000$, $\theta = \pi/4$, and $\lambda = 0$ (a), 0.03 (b), and 0.1 (c). The bold curves are the contour lines of $\omega_i = 0$ and enclose the linearly unstable regions. Only the bottom wall is superhydrophobic.

most unstable when the slip length is sufficiently small, whereas such a region is absent in plane Couette flow.

Figure 3 shows the effect of the slip on the eigenspectrum of 1D, 2D and 3D perturbation modes. The 1D mode $(\alpha, \beta) = (0, 0)$ is the least stable mode in the no-slip case, and figure 3(a) shows its eigenspectrum. The observation is that the eigenvalues of this mode stay purely imaginary as λ increases, and they all move toward 0 but stay negative. In other words, such perturbations will become less stable under the slip but stay linearly stable. No qualitative changes in the stability property are observed. Figure 3(b, c) show the eigenspectra of 2D modes $(\alpha, \beta) = (0, 3)$ and $(\alpha, \beta) = (0.1, 0)$, respectively. For the streamwise-independent mode $(\alpha, \beta) = (0, 3)$, the slip significantly changes the eigenspectrum. Besides destabilizing the leading eigenmode, the slip greatly changes the phase speed of the eigenmodes. In the no-slip case, the eigenvalues are imaginary and have zero streamwise and spanwise phase speeds. As λ increases, the real part of the eigenvalues becomes non-zero, i.e. the eigenmodes develop non-zero spanwise phase speeds, and the phase speeds appear to increase as λ increases. This can be expected because the slip induces a spanwise base-flow component, which increases as λ increases and will have an advective effect on the eigenmodes in the spanwise direction. On the contrary, the spanwise-independent mode $(\alpha, \beta) = (0.1, 0)$ only undergoes a slight quantitative change under the slip, see figure 3(c). Most eigenmodes are slightly destabilized by the slip, including the leading eigenmode, but there are ones that are stabilized, see the inset in panel (c). Although most of the eigenmodes become less stable, they all stay linearly stable even when λ is as large as 0.1. That $\beta = 0$ modes all stay linearly stable as λ increases can also be seen in figure 2. The spanwise phase speed of mode $(\alpha, \beta) = (0.1, 0)$ necessarily stays zero and the streamwise phase speed only increases very slightly under the slip. This is also expected because the advection by the W component of the base flow will not have an influence on the spanwise phase speed for spanwise independent flow structures, because a shift in the spanwise direction will not induce any phase change. The left part of the Y-shape spectrum, which corresponds to the wall modes near the bottom wall, is more affected than the right part of the spectrum, which corresponds to wall modes near the top wall.

The eigenspectrum of the 3-D mode $(\alpha, \beta) = (0.1, -3)$ also undergoes qualitative changes as λ increases, similar to the 2D mode $(\alpha, \beta) = (0, 3)$. Figure 3(d) shows that the eigenvalues of the no-slip case are all located below $\omega_i = 0$ and symmetrically about $\omega_r = 0$. Whereas, the eigenvalues move to the left and the left branch of the Y-shape spectrum is separated into two branches. The streamwise phase speed $|\omega_r/\alpha|$ can even be larger than the wall speed, which is attributed to the convective effect of the spanwise base-flow component and the smallness of $\arctan|\alpha/\beta|$ of the eigenmodes, see the illustration in figure 4(a). Similar phenomenon for small-α modes was reported for channel flow [18]. Besides, the centremodes

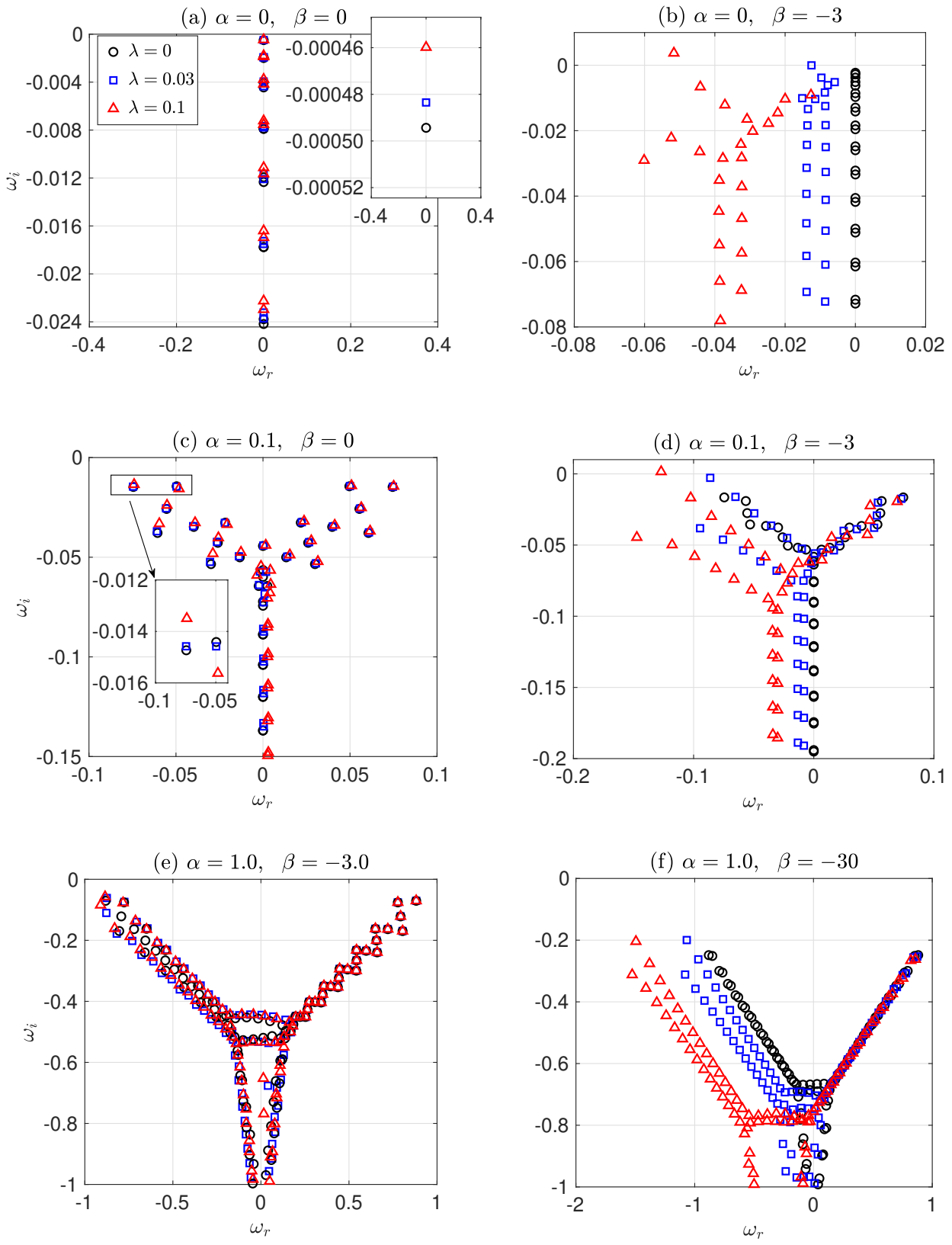

Figure 3: (a-f) The eigenspectrum of modes $(\alpha, \beta) = (0,\ 0)$, $(\alpha, \beta) = (0,\ 3)$, $(\alpha, \beta) = (0.1,\ 0)$, $(\alpha, \beta) = (0.1,\ -3)$, $(\alpha, \beta) = (1.0,\ -3)$, and $(\alpha, \beta) = (1.0,\ -30)$ for $Re = 5000$, $\theta = \pi/4$ and $k = 0.5$. The inset in panel (a) shows the zoom-in view of the least stable eigenmode. Only the bottom wall is slippery.

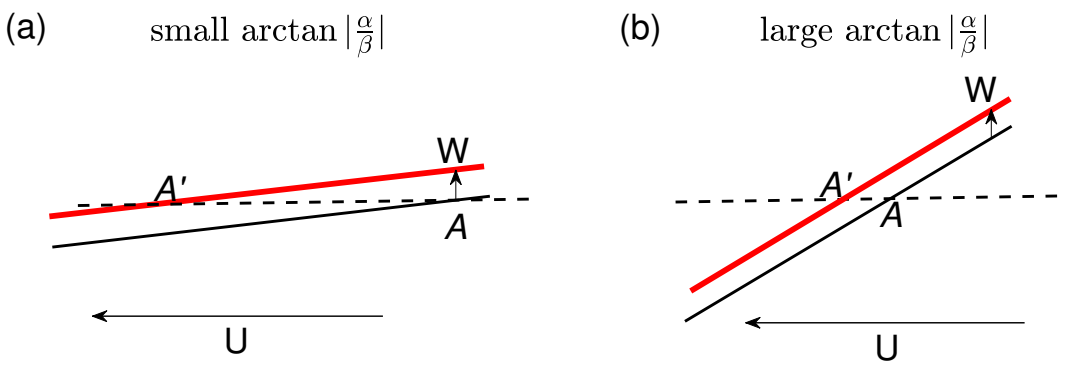

Figure 4: Illustration of the effect of W on the streamwise phase speed of the eigenmodes with $\alpha > 0$ and $\beta < 0$. Bottom wall is slippery, near which W is positive (see the vertical arrow) and U is negative (the horizontal arrow). Although W is small, a spanwise advection of the waves (from the thin black line to the red bold line) can cause a large shift in the streamwise direction (from A to A') if $\arctan|\frac{\alpha}{\beta}|$ is small (a), therefore, the spanwise advection could add on the streamwise advection by U, resulting in a streamwise phase speed larger than the wall speed. On the contrary, if $\arctan|\frac{\alpha}{\beta}|$ is large (b), the spanwise advection will have a much weaker effect on the streamwise phase speed and the advection of U will dominate.

also develop a non-zero phase speed because the slip on the bottom wall results in an asymmetry about y and a spanwise component in the base flow. The ω_i of the leading eigenmode changes from negative to positive, indicating the appearance of linear instability as λ becomes sufficiently large. The 3D mode $(\alpha, \beta) = (1.0, -3.0)$, which is outside of the linearly unstable region and has a relatively large $\arctan|\alpha/\beta|$, is only slightly affected, see figure 3(e) and 4(b). However, although the mode $(\alpha, \beta) = (1.0, -30.0)$ is also outside the linearly unstable region, the spectrum also undergoes significant changes in ω_r (see figure 3f), indicating significant changes in the streamwise phase speed, which can also be attributed to the smallness of $\arctan|\alpha/\beta|$ and the non-zero W, see the illustration in figure 4(b).

In summary, the slip mainly affects the eigenspectrum in two aspects. First, the slip can destabilize the modes with small α and relatively large $|\beta|$, including the streamwise independent modes. Second, the slip affects the phase speed of the modes with small $\arctan|\frac{\alpha}{\beta}|$ significantly, no matter the mode is inside the unstable region or not. The streamwise phase speed may either be larger than the wall speed or change its sign due to the smallness of $\arctan|\frac{\alpha}{\beta}|$ and the spanwise advection by W. The slip only has a slight effect on the spanwise-independent modes and the modes with large $\arctan|\alpha/\beta|$.

In the following, we will focus on the critical Reynolds number Re_{cr}, at which the instability first appears, and its dependence on the slip parameters.

3.2 The neutral curves

For fixed slip parameters, it takes scanning the three dimensional parameter space (Re, α, β) to obtain the neutral surface, at which the growth rate $\omega_i = 0$. This will be very expensive. Here, we choose to fix either α or β to compute the neutral curve in the Re-α plane or Re-β plane, and show the changes as the slip parameters change.

In figure 5, it can be seen that, as λ increases, the neutral curve moves towards smaller Re in all the cases, which indicates that a larger slip length destabilizes the flow more, as also shown in figure 2. For fixed $\beta = -1$ (panel a, c), instability is confined in the small-α regime even at high Reynolds numbers, see the turning down of the upper branch of the neutral curves for $\lambda = 0.03$ and 0.05 as Re increases, and the $\lambda = 0.01$ curve is likely of the same trend also, just the turning should happen at higher Re. Comparing $\theta = \pi/4$ and $\theta = \pi/8$, the former shows instability at lower Re and in a wider α region, indicating that the former destabilizes the flow more than the latter. This is consistent with former studies for channel

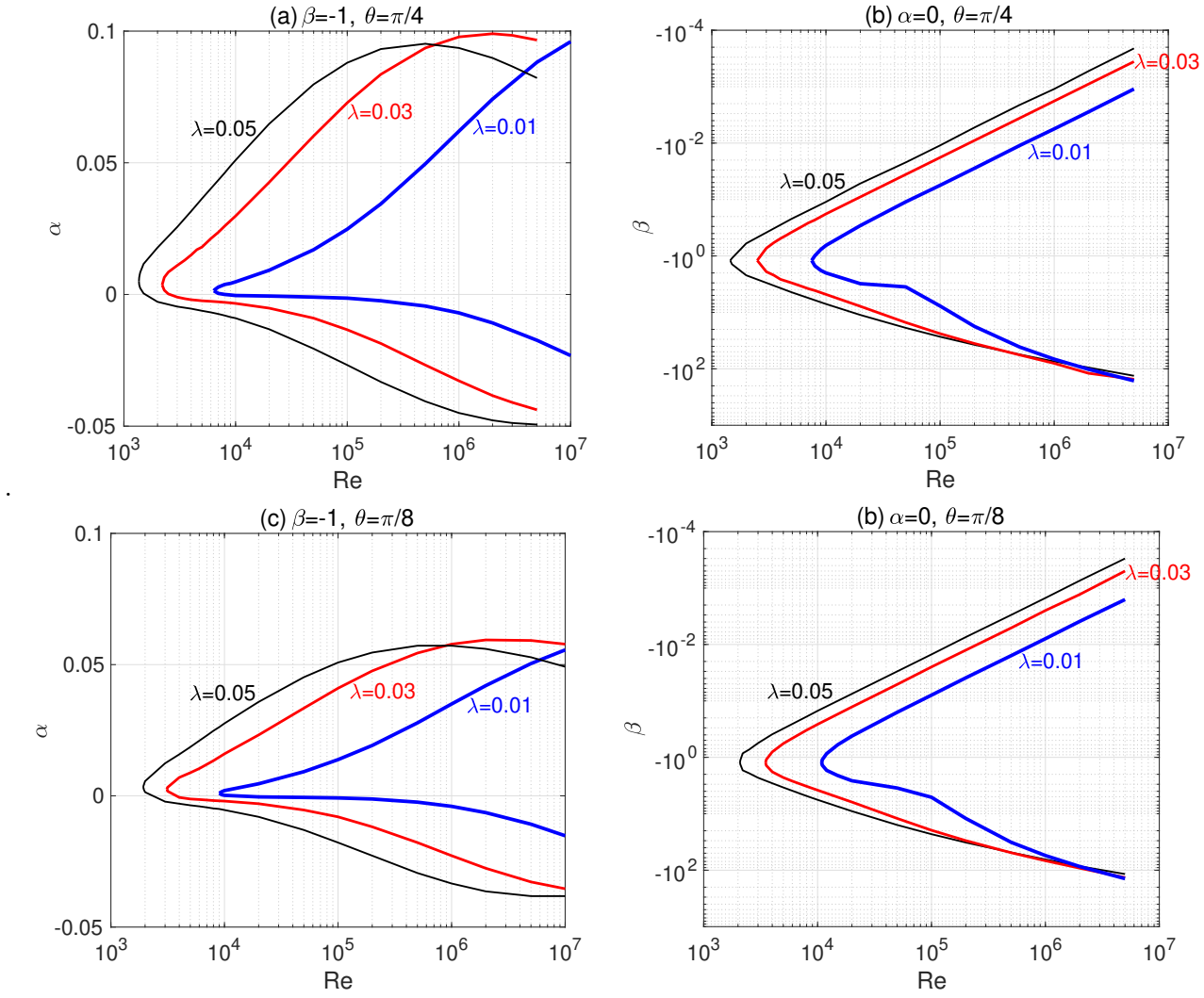

Figure 5: Neutral curves for fixed α or β, and their dependence on the slip length λ and the misalignment angle θ. (a) $\beta = -1$ and $\theta = \pi/4$. (b) $\alpha = 0$ and $\theta = \pi/4$. (c) $\beta = -1$ and $\theta = \pi/8$. (d) $\alpha = 0$ and $\theta = \pi/8$. For each case, $\lambda = 0.01$, 0.03 and 0.05 are considered.

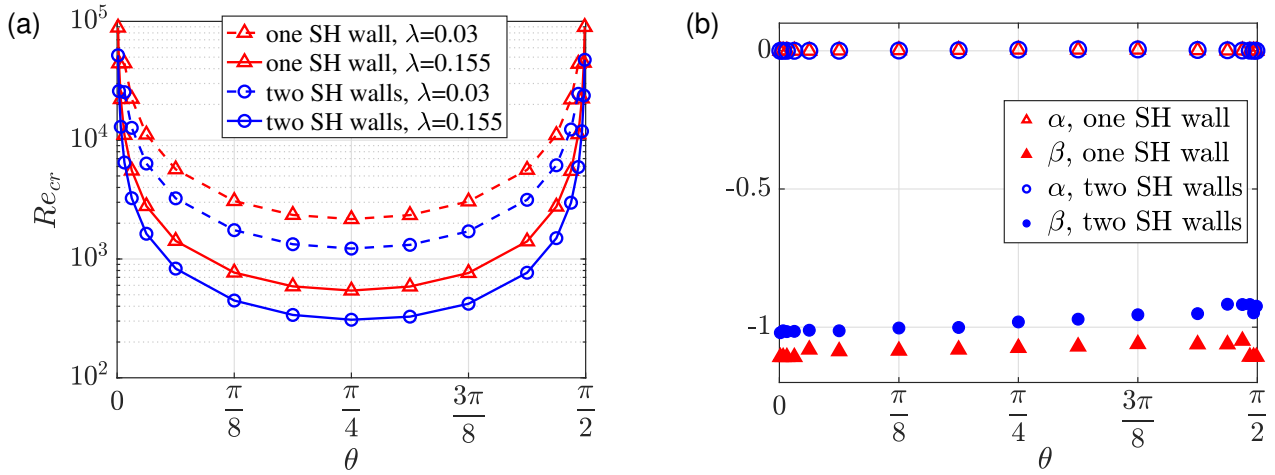

Figure 6: (a) The dependence of Re_{cr} on the misalignment angle θ for $\lambda = 0.03$ and 0.155. (b) The critical wavenumber as a function of θ. The value of α is very small, being $O(10^{-3})$ or smaller, and β is close to unity. The critical wavenumbers for the two slip lengths are close, and only those for $\lambda = 0.155$ are plotted to avoid crowding.

flow which reported that $\theta = \pi/4$ is close to the optimal angle [18, 23, 24]. In fact, later sections will show that $\theta = \pi/4$ is nearly optimal for destabilizing the plane Couette flow also.

For fixed $\alpha = 0$, the unstable β region keeps broadening as Re increases. The upper branch shows a $\beta \propto \frac{1}{Re}$ scaling for all the λ values considered. The lower branch is in a regime with $|\beta| \gg 1$, and the magnitude of β keeps increasing as Re increases and no sign of saturation is observed in the Re range we considered. But it should be noted that, results with very large β may be only illustrative for showing the trend, because the spanwise wavelength of the unstable wave, $2\pi/|\beta|$, will be very small and may become comparable with the widths of the microgrooves, which will make the homogenization of the slip effect invalid.

Another noticeable point is that, in each case, the noses of the neutral curves, i.e. the lowest Re for instability, appear at a nearly constant α (close to 0) or β (close to -1) for different λ values. This will be revisited in the following sections when the critical Reynolds number is investigated.

3.3 The critical Reynolds number Re_{cr}

3.3.1 Dependence on the misalignment angle θ

First, we show the dependence of Re_{cr} on the misalignment angle θ. It has been shown that the angle that has the strongest destabilizing effect is close to (slightly larger than) $\pi/4$ for channel flow [24], and the larger the λ, the larger the deviation from $\pi/4$. Figure 6(a) shows the dependence of the critical Reynolds number on θ for plane Couette flow. Both the one-SH-wall case and two-SH-walls case are shown. It can be seen that, for either case, Re_{cr} reaches its minimum approximately at $\pi/4$, even at large slip length of $\lambda = 0.155$. Different from channel flow where the Re_{cr} curve shows noticeable asymmetry about the most destabilizing θ, here, the Re_{cr} curve is nearly symmetric about $\theta = \pi/4$. This observation indicates that plane Couette flow is less sensitive to the slip-length ratio $k = 0.5$ than channel flow. In comparison, the two-SH-walls case always has a lower Re_{cr} than the one-SH-wall case for all θ values investigated. In channel flow, the two-SH-walls case gives a lower Re_{cr} also for most θ values except for the close vicinity of $\theta = 0$ where the one-SH-wall case may give a lower Re_{cr} [24]. This complexity for channel flow near $\theta = 0$ is attributed to the existence of the TS instability. Ref. [24] reported the following. At $\theta = 0$, compared to the two-SH-walls case, the TS mode is less stabilized by the slip in the one-SH-wall case because the other wall is no-slip and the TS mode is expected to be nearly unaffected near the no-slip

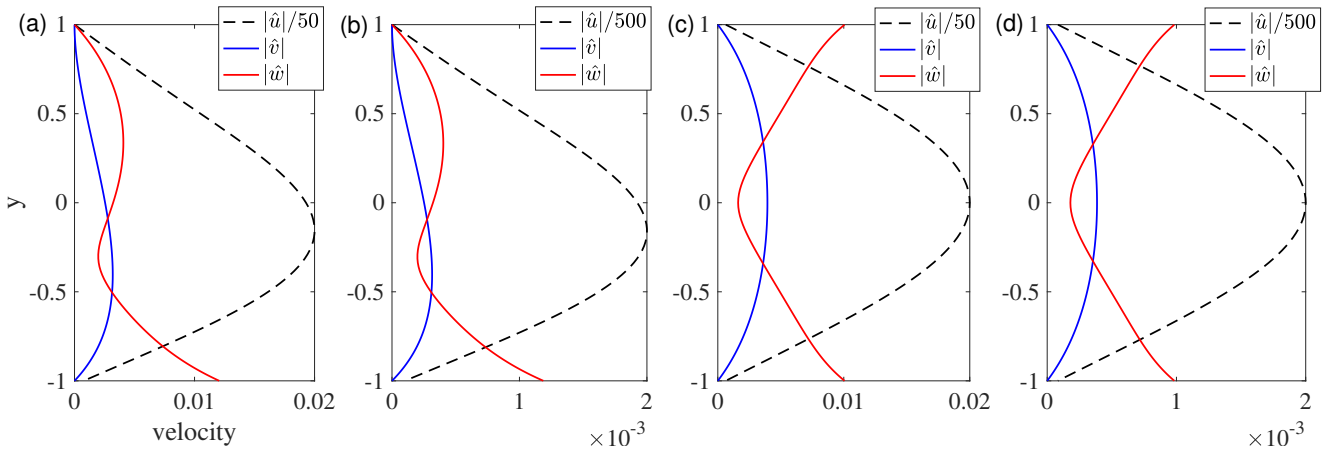

Figure 7: Eigenfunctions for large and small θ values at the critical Reynolds number. (a, b) One-SH-wall at $\theta = \pi/4$ and $\pi/64$, respectively. (c, d) Two-SH-walls at $\theta = \pi/4$ and $\pi/64$, respectively. Because u component is much larger than the other two, it is scaled properly for a better visualization, and v and w components are normalized by the maximum of their respective u component, i.e. $\max_y |\hat{u}|$. Other parameters are $\lambda = 0.03$ and $k = 0.5$ for all the cases.

wall. Whereas, the TS mode is greatly stabilized by the slip in the two-SH-walls case, resulting in a much higher Re_{cr} than the one-SH-wall case. As said above, there is no such TS instability in plane Couette flow so that there is no such complexity in plane Couette flow near $\theta = 0$.

Figure 6(b) shows the critical wavenumbers as θ changes. It can be seen that both α and β are nearly constant at the criticality. It is noted that α is very small, at $O(10^{-3})$ or even smaller, i.e. the leading eigenmodes are of structures that are nearly streamwise independent. This characteristic is similar to the unstable modes in slippery channel flow, termed as crossflow vortices in Ref. [23], and in the cross-flow instability of 3D boundary layer flow [34, 35]. The spanwise wavenumber β stays close to -1 for all θ values. Therefore, the flow structures are likely similar at different θ values, just as the similarities between the eigenfunctions indicate in figure 7 for $\theta = \pi/64$ and $\pi/4$. This point is different from channel flow, for which it was shown that the critical α and β at small θ values both undergo complex changes [24], indicating changes in the flow structures. This is also attributed to the switch between TS mode and superhydrophobic mode in channel flow in the small-θ regime.

Figure 8 shows the flow structure of the leading eigenmode at the critical Reynolds number for $\theta = \pi/4$ and $\lambda = 0.03$. In both cases, the flow structures nearly fill the whole gap between the two walls. The flow structure in the one-SH-wall case is slightly skewed toward the bottom wall (see figure 7(a,b) also). Both structures exhibit vortices and alternating high-speed and low-speed regions along the streamwise direction, and the two are highly similar to each other except for in the region close to the top wall, just as indicated by the similar eigenfunctions shown in figure 7.

Figure 9 shows Re_{cr} and the critical wavenumber in the small-θ regime. The results suggest a $Re_{cr} \propto \theta^{-1}$ scaling for both the one-SH-wall and two-SH-walls cases. This gives $Re_{cr} \to \infty$ as $\theta \to 0$. However, it should be noted that we have only explored Re up to $O(10^6)$ and θ down to $O(10^{-5})$, therefore, we cannot claim that this scaling still holds at higher Re or smaller θ. Nevertheless, if this scaling would indeed hold, it would suggest that any arbitrarily non-vanishing θ is sufficient to cause superhydrophobic instability, for both $\lambda = 0.03$ and $\lambda = 0.155$. The same scaling is also found in our data as $\theta \to \pi/2$, i.e. $Re_{cr} \propto (\pi/2 - \theta)^{-1}$ (not shown). These results also indicate that, without the misalignment, the slip-length ratio of $k = 0.5$ alone is not sufficient to destabilize the flow. Figure 9(b) shows that the critical wavenumber $\alpha_{cr} \propto \theta$ in the small-θ regime. Given that $Re_{cr} \propto \theta^{-1}$, we get $Re_{cr}\alpha_{cr} \approx$ const.. The critical β is nearly constant for both slip cases, which is about -1.1 for the one-SH-wall case and -1.01 for the two-SH-walls case.

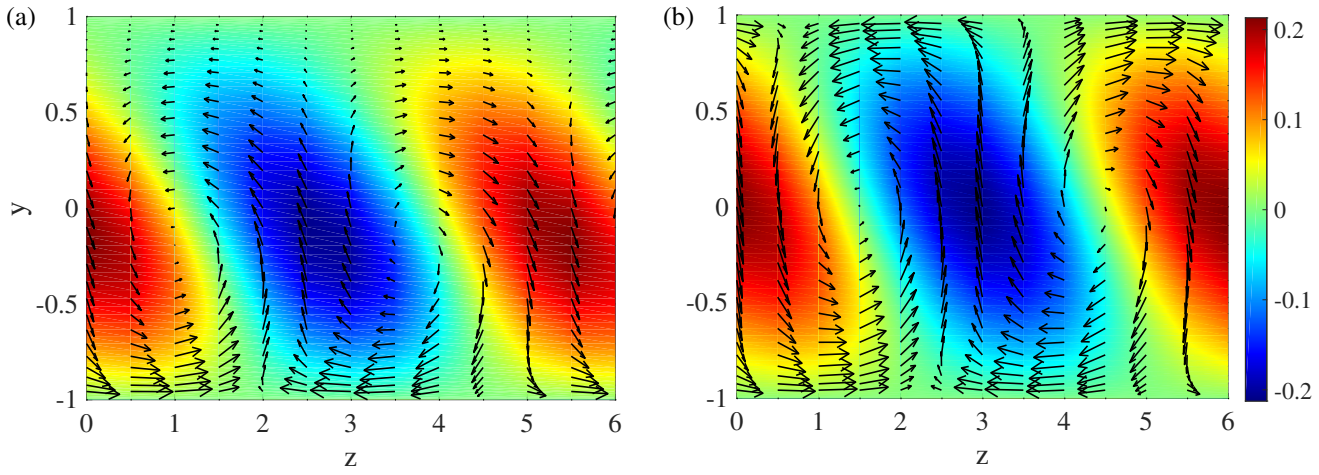

Figure 8: The flow structure of the leading eigenmode at the critical Reynolds number for $\theta = \pi/4$ and $\lambda = 0.03$. The color shows the streamwise velocity and the arrows show the velocity in the $z - y$ crosssection. (a) One SH wall at $Re = 2165$, $\alpha = 0.004$ and $\beta = -1.17$. (b) Two SH walls at $Re = 1223$, $\alpha = 0.004$ and $\beta = -1.07$.

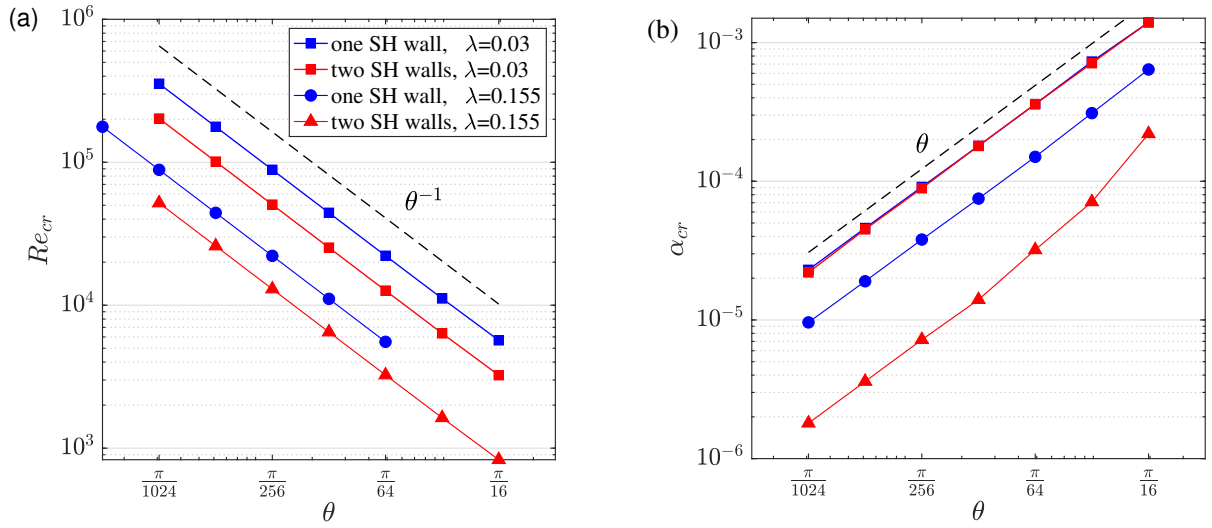

Figure 9: (a) The relationship between Re_{cr} and θ at small θ values. The dashed line is to show the $\propto \theta^{-1}$ scaling. (b) The scaling of the critical α with θ. The dashed line is to show the $\propto \theta$ scaling. The critical β is not shown, which is nearly constant of $\beta_{cr} \approx -1.1$ for the one-SH-wall case and -1.01 for the two-SH-walls case with $\lambda = 0.155$, and -1.17 and -1.09, respectively, with $\lambda = 0.03$.

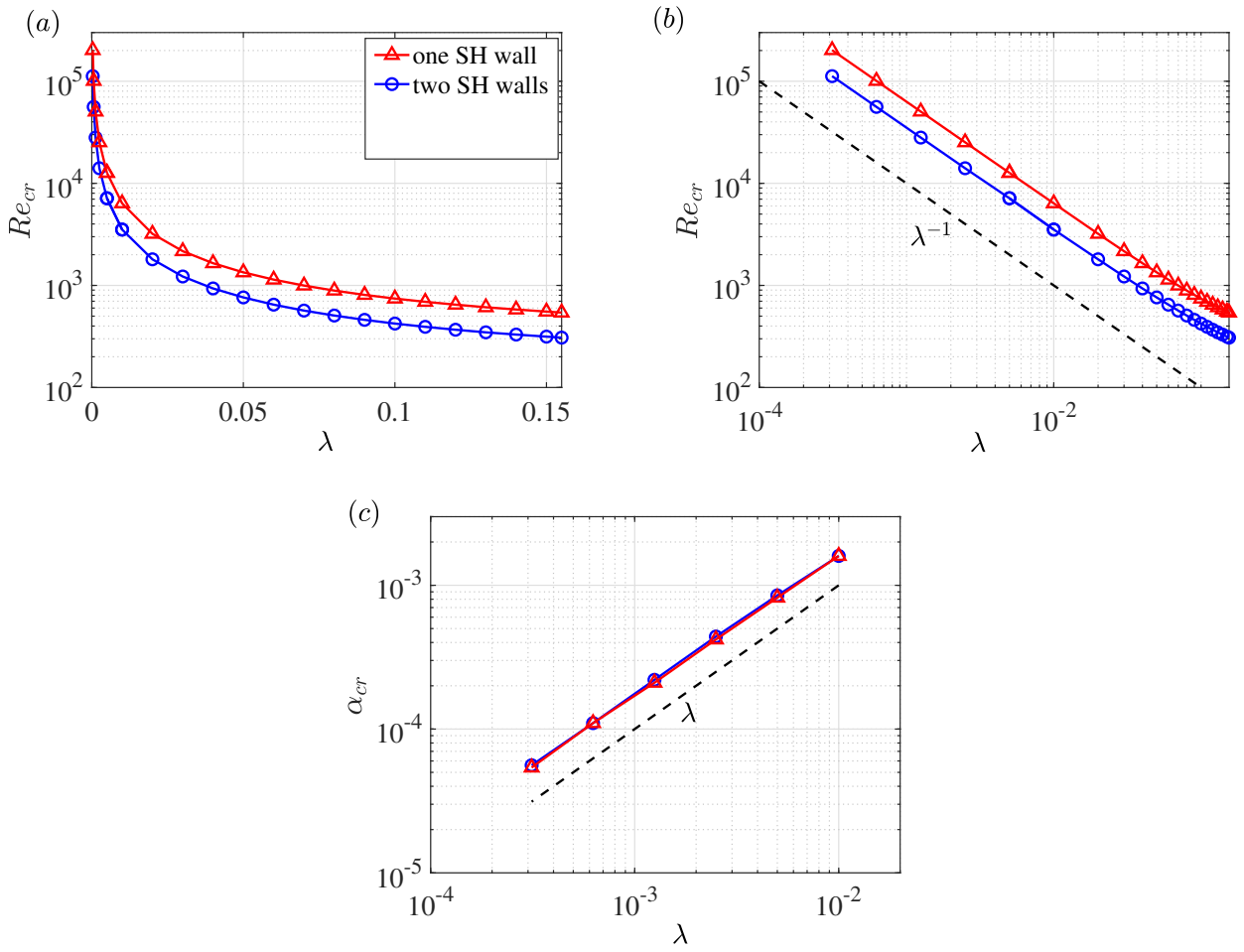

Figure 10: (a) The dependence of Re_{cr} on λ for $k = 0.5$ and $\theta = \pi/4$. (b) The same plot as in panel (a) in log-log scale to highlight the scaling of Re_{cr} with λ in the small-λ regime. The dashed line shows the λ^{-1} scaling. (c) The critical α in the small-λ regime. The dashed line shows the $\propto \lambda$ scaling. The critical β is nearly constant and not shown here, which is -1.18 in the one-SH-wall case and -1.1 in the two-SH-wall case.

3.3.2 Dependence on the slip length λ

Next, considering that $\theta = \pi/4$ nearly gives the lowest Re_{cr}, in the following, we fix $\theta = \pi/4$ and investigate the dependence of Re_{cr} on the slip length λ, see figure 10. The overall trend is that Re_{cr} decreases as λ increases, and the decrease is sharp when λ is small and slow when λ becomes large. The Re_{cr} can be reduced to a few hundred when λ is $O(10^{-1})$. In the whole λ range investigated, the two-SH-walls case always gives a lower Re_{cr} than the one-SH-wall case does.

In the small-λ regime, we find a $Re_{cr} \propto \lambda^{-1}$ scaling, see figure 9(b). This trend gives $Re_{cr} \to \infty$ as $\lambda \to 0$, which is consistent with the fact that the no-slip plane Couette flow is linearly stable at arbitrary Re. It can be seen that the relationship deviates from this scaling above $\lambda \simeq 0.01$. An implication of this λ^{-1} scaling is that, surprisingly, any arbitrarily small slip length can make the flow linearly unstable, at least for $\theta = \pi/4$ and $k = 0.5$. Figure 9(c) shows the scaling of the critical streamwise wavenumber, which is nearly $\propto \lambda$, which indicates that $Re_{cr}\alpha_{cr} \approx$ const., whereas the critical spanwise wavenumber stays nearly constant, being -1.18 in the one-SH-wall case and -1.1 in the two-SH-wall case.

In the following, we discuss about the scaling of Re_{cr} in the small-parameter regime. We take the

θ	λ	k	Re_{cr}	α	β
$\frac{\pi}{4}$	0.00125	0.5	28046	0.00021	-1.103
$\frac{\pi}{4}$	0.01	0.936403	28017	0.00020	-1.086
$\frac{\pi}{4}$	0.05	0.986254	28583	0.00013	-1.039
$\frac{\pi}{4}$	0.1	0.992457	30012	0.00006	-0.991
$\frac{\pi}{64}$	0.01	0.354904	28231	0.00019	-1.105
$\frac{\pi}{64}$	0.05	0.860594	28685	0.00013	-1.047
$\frac{\pi}{64}$	0.1	0.923525	30050	0.000059	-0.999

Table 1: Different slip parameters ($\theta,\ \lambda,\ k$) that give identical $W = 3.12 \times 10^{-4} y$ and the corresponding Re_{cr}. The data is from the two-SH-wall case.

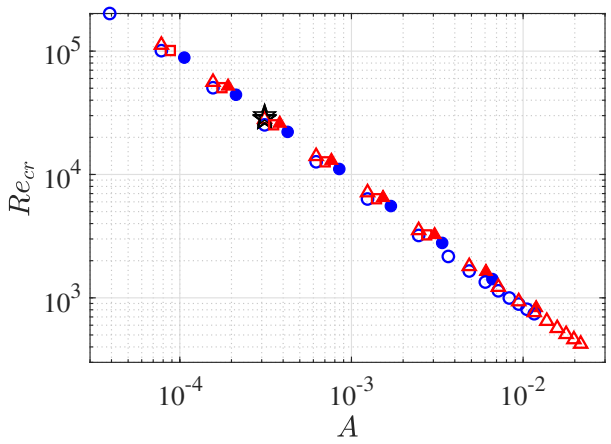

Figure 11: (a) The dependence of Re_{cr} on the prefactor A in W. The data from figure 9 are plotted as open symbols, data from figure 10(b) are plotted as filled symbols, and data from table 1 are plotted as pentagrams.

two-SH-walls case for an example. It is noticed that, for fixed slip length λ, k (excluding $k = 1$) and y, in the limit of $\theta \to 0$, we have

$$W(y) = \frac{(1-k)\lambda \sin\theta\cos\theta}{(k\lambda+1)(\lambda+1)} y \sim \sin 2\theta \sim \theta. \tag{14}$$

Similarly, for fixed k (excluding $k = 1$), θ and y, in the limit of $\lambda \to 0$, we have

$$W(y) = \frac{(1-k)\lambda \sin\theta\cos\theta}{(k\lambda+1)(\lambda+1)} y \sim \lambda. \tag{15}$$

Based on these observations, if denoting the prefactor in the expression of $W(y)$ as A, i.e. denoting $W(y) = Ay$, then the above two relationships seem to suggest that

$$Re_{cr} \propto A^{-1} \tag{16}$$

in the limit of $A \to 0$, which can be realized by either $\theta \to 0$ or $\lambda \to 0$. The nonvanishing W is a result of the anisotropy of the slip combined with the misalignment of the microgrooves with the wall motion, and to some extent, W or the prefactor A can be considered as the 'strength' of the overall slip effect. Then this implies an inverse relationship between Re_{cr} and the 'strength' of the slip effect, and that an arbitrarily small slip effect can lead to linear instability.

To verify the relationship (16), we calculate Re_{cr} at different slip parameters that give identical A. Table 1 shows the parameters (θ, λ, k) we have considered, which give $A = 3.12 \times 10^{-4}$, and the

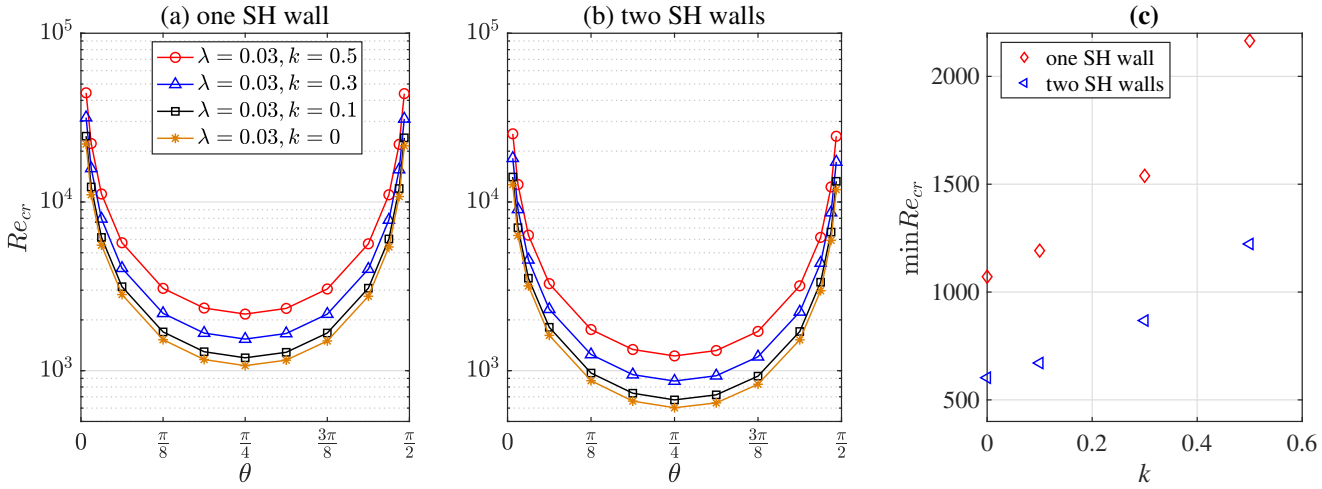

Figure 12: The dependence of Re_{cr} on the slip length ratio k. The slip length is fixed at $\lambda = 0.03$ for all ratios. (a) One SH wall. (b) Two SH walls. The lowest Re_{cr} achieved (approximately at $\theta = \pi/4$) is plotted against k in panel (c).

corresponding Re_{cr}, critical wavenumbers α and β. The parameters are arbitrarily selected, including both large values and small values, but the Re_{cr}'s turn out to be very close to each other. This seems to support our argument that Re_{cr} is approximately determined by the prefactor A when A is sufficiently small. To show the dependence of Re_{cr} on A, we collect data from figure 9(a) , figure 10(b) and table 1 and plot them together in figure 11. It can be seen that each data set supports the $Re_{cr} \propto A^{-1}$ scaling, and furthermore, all data sets are quite close to each other, although a complete collapse is not obtained. This suggests that Re_{cr} indeed can be approximately determined by A in the small-parameter regime, disregarding the specific parameter setting.

3.3.3 Dependence on the slip length ratio k

Third, we investigate the influence of the anisotropy, quantified by the slip length ratio k, on the critical Reynolds number. So far, only $k = 0.5$ is studied systematically. This ratio is suggested by a few theoretical modelings by assuming flat and rigid gas-liquid interfaces with free-slip boundary condition on the interfaces [28, 29, 42]. Nevertheless, some studies suggested that this ratio can be smaller if the fluid is allowed to partially intrude into the grooves, which can significantly reduce the effective transverse slip length of the microgrooves so that reduce the ratio [43]. We consider smaller ratios of $k = 0.3$, 0.1 and 0, and compare them with $k = 0.5$, see figure 12. The results show that as k decreases, Re_{cr} monotonically decrease in all the cases investigated. The lowest Re_{cr} at $\theta = \pi/4$ can be reduced to approximately 200 in the two-SH-walls case with $k = 0$. This trend suggests that Re_{cr} can be reduced further if k can be reduced further, but smaller ratios may not be realized easily in experiments. It is noticed that Re_{cr} only reduces slightly from $k = 0.1$ to 0. This dependence on the ratio k is similar to channel flow [24]. The difference is that, here, even at the limiting case of $k = 0$, the Re_{cr} curve is still nearly symmetric about $\theta = \pi/4$, whereas there is significant asymmetry and the θ giving the minimum Re_{cr} is significantly larger than $\theta = \pi/4$ in channel flow. Again, this further indicates a less sensitivity on the slip anisotropy for plane Couette flow.

3.3.4 Influence of the parallelism of microgrooves on the two walls

Following Ref. [24], here we also investigate the stability of the flow with different misalignment angles θ on the two walls. We do not intend to systematically calculate Re_{cr} as we did above, instead, starting from the $\min Re_{cr} = 1223$ at $\theta = 45°$ with $\lambda = 0.03$ and $k = 0.5$, we change θ on the bottom wall and

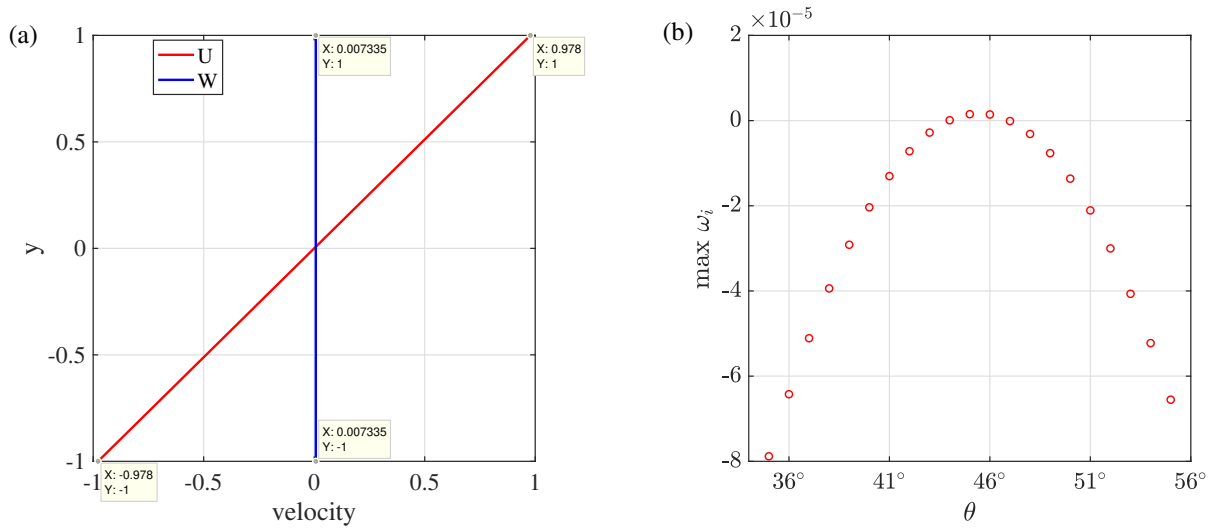

Figure 13: The influence of different θ on the two walls. (a) The base flow for the case with $\theta = 45°$ on the top wall and $-45°$ on the bottom wall. (b) The maximum growth rate $\max \omega_i$ as the bottom θ changes. The top θ is fixed at 45°, and other parameters are $Re = 1223$, $\lambda = 0.03$ and $k = 0.5$.

calculate the largest growth rate $\max \omega_i$ while fixing $\theta = 45°$ on the top wall. Figure 13(a) shows the base flow of the special case of $\theta = 45°$ on the top wall and $-45°$ on the bottom wall. It can be seen that, in this special case, the spanwise base flow W is independent of y, and U is identical to the case with equal θ on both walls. Figure 13(b) shows $\max \omega_i$ as the bottom θ changes around 45°. Clearly, $\max \omega_i$ reaches the maximum when $\theta = 45°$ on the bottom wall, which indicates that the case with equal θ on the two walls is more unstable or less stable than the case with different θ's. Particularly, the $\max \omega_i$ of the case shown in panel (a) is -0.0017, i.e. when $\theta = -45°$ on the bottom wall, which is much lower than the $\max \omega_i$ of those θ values close to 45° shown in panel (b). Therefore, if instability is favored in the flow, the microgrooves on the two walls should be parallel to each other because differing θ's would result in a lower growth rate (i.e. higher stability). This conclusion is similar to the channel-flow case [24].

3.4 Energy budget analysis

Energy budget analysis was shown to be able to reveal the destabilizing mechanism in parallel shear flows of both miscible and immiscible fluids that involve viscosity stratification or interfaces [16, 17, 44, 45]. In order to further analyze the instability of the flow in concern, we also performed an energy budget analysis. The energy budget equation reads

$$\dot{E} := \frac{\partial}{\partial t} \int_V \boldsymbol{u}^2 \mathrm{d}V = P - \epsilon + \Pi, \tag{17}$$

where P, ϵ and Π are defined as

$$P = -\int_V \left[uv \frac{\mathrm{d}U}{\mathrm{d}y} + wv \frac{\mathrm{d}W}{\mathrm{d}y} \right] \mathrm{d}V, \tag{18}$$

$$\epsilon = \frac{1}{Re} \int_V \left[\left(\frac{\partial \boldsymbol{u}}{\partial x} \right)^2 + \left(\frac{\partial \boldsymbol{u}}{\partial y} \right)^2 + \left(\frac{\partial \boldsymbol{u}}{\partial z} \right)^2 \right] \mathrm{d}V, \tag{19}$$

$$\begin{aligned} \Pi = \frac{1}{Re} \int_0^{2\pi/\alpha} \int_0^{2\pi/\beta} [& u(x,1,z) \frac{\partial u(x,1,z)}{\partial y} - u(x,-1,z) \frac{\partial u(x,-1,z)}{\partial y} \\ & + w(x,1,z) \frac{\partial w(x,1,z)}{\partial y} - w(x,1,z) \frac{\partial w(x,1,z)}{\partial y}] \mathrm{d}x \mathrm{d}z. \end{aligned} \tag{20}$$

λ	α	β	$\dot{E}$	P_U	P_W	ϵ	Π
0	0.0046	-1.1	-0.0055	0	0	0.0055	0
0.02	0.0046	-1.1	-0.0033	0.0022	-2.6842×10^{-9}	0.0054	-9.4011×10^{-5}
0.04	0.0046	-1.1	-0.0012	0.0044	6.4487×10^{-8}	0.0055	-1.6745×10^{-4}
0.06	0.0046	-1.1	3.2261×10^{-4}	0.0063	1.2992×10^{-7}	0.0058	-2.2825×10^{-4}
0.08	0.0046	-1.1	0.0012	0.0078	-3.6691×10^{-8}	0.0063	-2.8363×10^{-4}

Table 2: Energy budget of the leading eigenmode for a few parameters across the stability boundary. The Reynolds number $Re = 700$, $\theta = \pi/4$, and wavenumbers are fixed while λ is increased such that the flow changes from being stable to unstable. The kinetic energy production due to the streamwise base flow U, $P_U = -\int_V uv\frac{\mathrm{d}U}{\mathrm{d}y}\mathrm{d}V$, and due to the spanwise base flow W, $P_W = -\int_V wv\frac{\mathrm{d}W}{\mathrm{d}y}\mathrm{d}V$, are calculated separately. All terms are normalized by the kinetic energy E.

Re	α	β	$\dot{E}$	P_U	P_W	ϵ	Π
300	0.004	-1	-0.0034	0.0080	1.6361×10^{-6}	0.0105	-8.4128×10^{-4}
400	0.004	-1	-4.9081×10^{-4}	0.0085	1.2405×10^{-7}	0.0084	-6.0612×10^{-4}
500	0.004	-1	9.4153×10^{-4}	0.0087	7.7030×10^{-7}	0.0072	-4.7115×10^{-4}
600	0.004	-1	0.0016	0.0086	2.8530×10^{-7}	0.0066	-3.8662×10^{-4}

Table 3: Energy budget of the leading eigenmode for a few parameters across the stability boundary. $\lambda = 0.1$, $\theta = \pi/4$, and wavenumbers are fixed while Re is increased such that the flow changes from being stable to unstable. The definitions of all terms are the same as those in table 2.

As usual, P measures the extraction rate of kinetic energy by disturbances from the base flow, ϵ measures the viscous dissipation rate. Different from the no-slip case, an extra contribution to the energy production rate by the spanwise base flow W appears in P (see equation (18)), and an extra term Π appears which measures the contribution of the nonvanishing slip velocities the wall boundary (see equation (20)).

The results are shown in table 2 and 3. It can be seen that the production of kinetic energy is mainly attributed to the part P_U. The production due to the spanwise velocity P_W is orders of magnitude smaller than P_U. This is because W is much smaller than U and the spanwise perturbation w is also much smaller than the streamwise perturbation u, as shown in figure 7. Therefore, P_W cannot be responsible for the destabilization, and in other words, the cross-flow component of the spanwise base flow W does not directly contribute to the observed instability. The contribution from the slip velocity Π is much larger than P_W, but still significantly smaller than P_U. Besides, for all the parameters considered, Π is negative, which suggests that the velocity slip on the walls does not directly destabilize the flow either but plays a stabilizing role. When Re, α and β are fixed while λ is increased (see table 2), the energy dissipation only changes slightly, whereas the production P_U increases significantly until it outweighs dissipation so that the flow becomes unstable. When λ, α and β are fixed while Re is increased (see table 3), the production P_U changes little, whereas the dissipation decreases significantly until being outweighed by P_U so that the flow becomes unstable.

4 Conclusion

We studied the linear stability of plane Couette flow subject to an anisotropic slip boundary condition which models the effective slip effects of microgrooves that can have a misalignment about the direction of wall motion. We focused on the effects of the slip on the eigenspectrum and on the critical Reynolds number at which linear instability first appears.

The slip can significantly affect the growth rate and phase speed of the modes with small α and large $|\beta|$, including the $\alpha = 0$ modes, and render the flow linearly unstable. The slip can also significantly affect

the streamwise phase speed of the modes with small $\arctan|\frac{\alpha}{\beta}|$ that are not destabilized by the slip. We have illustrated that the significant change in the streamwise phase speed is due to the spanwise base-flow induced by the slip and the smallness of $\arctan|\frac{\alpha}{\beta}|$. The eigenmodes with large $\arctan|\frac{\alpha}{\beta}|$ and with $\beta = 0$ are not significantly affected by the slip in either growth rate or streamwise phase speed.

The critical Reynolds number Re_{cr} is very sensitive to the misalignment and the angle $\pi/4$ nearly results in the lowest Re_{cr}. In all parameter ranges investigated, the unstable mode at the critical Reynolds number is nearly streamwise-independent given $\alpha_{cr} \ll 1$, and the two-SH-wall setting always gives a lower Re_{cr} than the one-SH-wall setting. By fixing other parameters, Re_{cr} monotonically decreases as the slip length λ increases. Unlike channel flow, because of the absence of TS instability in plane Couette flow, there is no complexity due to the competition between the TS and superhydrophobic instabilities at small values of θ and λ. This allows us to study the scaling laws at small parameters, and the results show $Re_{cr} \propto \theta^{-1}$ and $Re_{cr} \propto \lambda^{-1}$. These scaling laws suggest that instability can be induced by arbitrary non-vanishing misalignment and slip length. Besides, our data show that $\alpha_{cr} \propto \theta$ and $\alpha_{cr} \propto \lambda$ in the small parameter regime, indicating $Re_{cr}\alpha_{cr} \approx$ const., whereas β_{cr} is nearly constant and close to -1. We further identified an inverse relationship between Re_{cr} and the prefactor in the expression of $W(y)$ (involving θ, λ and k), which we proposed as a compound measure of the strength of the slip effect. Similar to the channel flow, a larger slip length ratio k, which means stronger anisotropy in the slip effect, can result in a lower critical Reynolds number. The lowest Re_{cr} obtained is $O(10^2)$ when the slip length is increased to $O(0.1)$. For the two-SH-walls case, the flow is most unstable or least stable when the misalignment angles on the two walls are equal.

The energy budget analysis indicates that, aside from the production and dissipation terms as in the no-slip case, contributions from the spanwise base flow and nonvanishing slip velocities on the wall appear. However, the contribution from the spanwise base flow is very small and negligible, whereas the slip velocities at the wall tend to stabilize the flow for the parameters we investigated. At least from the point of view of the energy budget, both the spanwise base flow component and the slip velocities at the wall do not directly contribute to the instability. Therefore, it can be inferred that the slip must affect the stability by affecting the production and dissipation in the bulk flow.

Although there are differences between plane Couette flow and channel flow due to the distinct base flows and stability properties in the no-slip case, our results show a high similarity of the slip effects on the superhydrophobic stability as well as in the flow structures of the unstable modes. Therefore, it can be inferred that this anisotropic slip boundary condition has a general destabilizing effects on wall-bounded shear flows and can cause linear instability at low Reynolds numbers. This destabilizing effect can be utilized to induce instability and asymmetry for flow controls, which may be useful for mixing-rate enhancement in low-Reynolds-number flows and flow-based particle sorting.

Acknowledgements

The authors acknowledge financial support from the National Natural Science Foundation of China under grant numbers 12322209 and 12272264. The work is also supported by "The Fundamental Research Funds for the Central Universities, Peking University". Discussion with Prof. Ming Dong is highly acknowledged.

Data availability

The data that support the findings of this study are available from the corresponding author upon reasonable request.

References

[1] J. Qu and J. P. Rothstein. Direct velocity measurements of the flow past drag-reducing ultrahydrophobic surfaces. *Phys. Fluids*, 17:103606, 2005.

[2] C. H. Choi and C. J. Kim. Large slip of aqueous liquid flow over a nanoengineered superhydrophobic surface. *Phys. Rev. Lett.*, 96:066001, 2006.

[3] C. Lee, C.-H. Choi, and C.-J Jim. Structured surfaces for a giant liquid slip. *Phys. Rev. Lett.*, 101:064501, 2008.

[4] C. Lee and C.-J Jim. Maximizing the giant liquid slip on superhydrophobic microstructures by nanostructuring their sidewalls. *Langmuir*, 25:12812, 2009.

[5] R. S. Voronov, D. V. Papavassiliou, and L. L. Lee. Review of fluid slip over superhy-drophobic surfaces and its dependence on the contact angle. *Industr. Eng. Chem. Res.*, 47:2455–2477, 2008.

[6] J. P. Rothstein. Slip on superhydrophobic surfaces. *Annu. Rev. Fluid Mech.*, 42:89–109, 2010.

[7] G. Chattopadhyay, K. C. Sahu, and R. Usha. Spatio-temporal instability of two superposed fluids in a channel with boundary slip. *International Journal of Multiphase Flow*, 113:264–278, 2018.

[8] Jr. J. M. Gersting. Hydrodynamic instability of plane porous slip flow. *Phys. Fluids*, 17:2126–2127, 1974.

[9] A. Kwang-Hua Chu. Instability of navier slip flow of liquids. *C. R. Mechanique*, 332:895–900, 2004.

[10] E. Lauga and C. Cossu. A note on the stability of slip channel flows. *Phys. Fluids*, 17:088106, 2005.

[11] T. Min and J. Kim. Effects of hydrophobic surface on stability and transition. *Phys. Fluids*, 17:108106, 2005.

[12] K. C. Sahu, A. Sameen, and R. Govindarajan. The relative roles of divergence and velocity slip in the stability of plane channel flow. *Eur. Phys. J. Appl. Phys.*, 44:101–107, 2008.

[13] Vit Průsa. On the influence of boundary condition on stability of Hagen-Poiseuille flow. *Computers and Mathematics with Applications*, 57:763–771, 2009.

[14] S. Ghosh, R. Usha, and K. C. Sahu. Double-diffusive two-fluid flow in a slippery channel: A linear stability analysis. *Phys. Fluids*, 26:127101, 2014.

[15] S. Ghosh, R. Usha, and K. C. Sahu. Linear stability analysis of miscible two-fluid flow in a channel with velocity slip at the walls. *Phys. Fluids*, 26:014107, 2014.

[16] S. Ghosh, R. Usha, and K. C. Sahu. Absolute and convective instabilities in double-diffusive two-fluid flow in a slippery channel. *Chemical Engineering Science*, 134:1–11, 2015.

[17] G. Chattopadhyay, R. Usha, and K. C. Sahu. Core-annular miscible two-fluid flow in a slippery pipe: A stability analysis. *Phys. Fluids*, 29:097106, 2017.

[18] J. O. Pralits, E. Alinovi, and A. Bottaro. Stability of the flow in a plane microchannel with one or two superhydrophobic walls. *Phys. Rev. Fluids*, 2:013901, 2017.

[19] C. Chai and B. Song. Stability of slip channel flow revisited. *Phys. Fluids*, 31:084105, 2019.

[20] F. Picella, J. C. Robinet, and S. Cherubini. Laminar–turbulent transition in channel flow with superhydrophobic surfaces modelled as a partial slip wall. *J. Fluid Mech.*, 881:462–497, 2019.

[21] B. Liu and Y. Zhang. A numerical study on the natural transition locations in the flat-plate boundary layers on superhydrophobic surfaces. *Phys. Fluids*, 32:124103, 2020.

[22] K. Chen and B. Song. Linear stability of slip pipe flow. *J. Fluid Mech.*, 910:A35, 2021.

[23] A. Jouin, S. Cherubini, and J. C. Robinet. Turbulent transition in a channel with superhydrophobic walls: the effect of roughness anisotropy. *J. Fluid Mech.*, 980:A49, 2024.

[24] X. Zhai, K. Chen, and B. Song. Linear instability of channel flow with microgroove-type anisotropic superhydrophobic walls. *Phys. Rev. Fluids*, 8:023901, 2023.

[25] J. Seo and A. Mani. On the scaling of the slip velocity in turbulent flows over superhydrophobic surfaces. *Phys. Fluids*, 28:025110, 2016.

[26] E. A. Davis and J. S. Park. Dynamics of laminar and transitional flows over slip surfaces: effects on the laminar–turbulent separatrix. *J. Fluid Mech.*, 894:A16, 2020.

[27] X. Xiong and J. Tao. Linear stability and energy stability of plane poiseuille flow with isotropic and anisotropic slip boundary conditions. *Phys. Fluids*, 32:094104, 2020.

[28] E. S. Asmolov and O. I. Vinogradova. Effective slip boundary conditions for arbitrary one-dimensional surfaces. *J. Fluid Mech.*, 706:108–117, 2012.

[29] E. Lauga and H. A. Stone. Effective slip in pressure-driven stokes flow. *J. Fluid Mech.*, 489:55–77, 2003.

[30] O. I. Vinogradova. Slippage of water over hydrophobic surfaces. *Int. J. Min. Process*, 56:31–60, 1999.

[31] K. H. Yu, C. J. Teo, and B. C. Khoo. Linear stability of pressure-driven flow over longitudinal superhydrophobic grooves. *Phys. Fluids*, 28:022001, 2016.

[32] S. D. Tomlinson and D. T. Papageorgiou. Linear instability of lid- and pressure-driven flows in channels textured with longitudinal superhydrophobic grooves. *J. Fluid Mech.*, 932:A12, 2022.

[33] F. Picella, J.-Ch. Robinet, and S. Cherubini. On the influence of the modelling of superhydrophobic surfaces on laminar–turbulent transition. *J. Fluid Mech.*, 901:A15, 2020.

[34] W. S. Saric, J. A. Hoos, and R. H. Radeztsky. Boundary-layer receptivity of sound with roughness. *Boundary Layer Stability and Transition to Turbulence (ASME, New York)*, 114:17–22, 1991.

[35] W. S. Saric, H. L. Reed, and E. B. White. Three dimensional boundary layers. *Ann. Rev. Fluid Mech.*, 35:413–440, 2003.

[36] V. A. Romanov. Stability of plane-parallel couette flow. *Functional Anal. i Prolożen*, 7:62–73, 1973.

[37] P. G. Drazin and W. H. Reid. *Hydrodynamic stability (Cambridge Mathematical Library)*. Cambridge University press, 2004.

[38] S. Bottin and H. Chaté. Statistical analysis of the transition to turbulence in plane couette flow. *Eur. Phys. J. B*, 6:143–155, 1998.

[39] Y. Duguet, P. Schlatter, and D. S. Henningson. Formation of turbulent patterns near the onset of transition in plane couette flow. *J. Fluid Mech.*, 650:119–129, 2010.

[40] L. N. Trefethen. *Spectral methods in Matlab*. SIAM, 2000.

[41] E. Yariv. Highly singular slip length for longitudinal shear flow over a dense bubble mattress. *J. Fluid Mech.*, 967:R3, 2023.

[42] J. R. Philip. Flows satisfying mixed no-slip and no-shear conditions. *Z. Andew. Math. Phys.*, 23:353, 1972.

[43] C-O Ng and C. Y. Wang. Stokes shear flow over a grating: Implications for superhydrophobic slip. *Phys. Fluids*, 21:013602, 2009.

[44] H. H. Hu and D. Joseph. Lubricated pipelining: stability of core-annular flow. part 2. *J. Fluid Mech.*, 205:359–396, 1989.

[45] R. Govindarajan and Sahu K. C. Instabilities in viscosity-stratified flow. *Ann. Rev. Fluid Mech.*, 46:331–353, 2014.